A cell–ECM mechanism for connecting the ipsilateral eye to the brain

Jianmin Su[a], Ubadah Sabbagh[a,b,1], Yanping Liang[a,1], Lucie Olejníková[a,c], Karen G. Dixon[d], Ashley L. Russell[e,f], Jiang Chen[a], Yuchin Albert Pan[a,g,h], Jason W. Triplett[d,e,f], and Michael A. Fox[a,i,j,k,2]

[a]Center for Neurobiology Research, Fralin Biomedical Research Institute at Virginia Tech Carilion, Roanoke, VA 24016; [b]Graduate Program in Translational Biology, Medicine, and Health, Virginia Tech, Blacksburg, VA 24061; [c]Department of Experimental Neurobiology, National Institute of Mental Health, Klecany 250 67, Czech Republic; [d]Center for Neuroscience Research, Children's National Medical Center, Washington, DC 20010; [e]Department of Pediatrics, The George Washington University School of Medicine and Health Sciences, Washington, DC 20052; [f]Department of Pharmacology & Physiology, The George Washington University School of Medicine and Health Sciences, Washington, DC 20052; [g]Department of Biomedical Sciences and Pathobiology, Virginia-Maryland College of Veterinary Medicine, Virginia Tech, Blacksburg, VA 24061; [h]Department of Psychiatry and Behavioral Medicine, Virginia Tech Carilion School of Medicine, Roanoke, VA 24016; [i]School of Neuroscience, Virginia Tech, Blacksburg, VA 24061; [j]Department of Biological Sciences, Virginia Tech, Blacksburg, VA 24061; and [k]Department of Pediatrics, Virginia Tech Carilion School of Medicine, Roanoke, VA 24016

Information about features in the visual world is parsed by circuits in the retina and is then transmitted to the brain by distinct subtypes of retinal ganglion cells (RGCs). Axons from RGC subtypes are stratified in retinorecipient brain nuclei, such as the superior colliculus (SC), to provide a segregated relay of parallel and feature-specific visual streams. Here, we sought to identify the molecular mechanisms that direct the stereotyped laminar targeting of these axons. We focused on ipsilateral-projecting subtypes of RGCs (ipsiRGCs) whose axons target a deep SC sublamina. We identified an extracellular glycoprotein, Nephronectin (NPNT), whose expression is restricted to this ipsiRGC-targeted sublamina. SC-derived NPNT and integrin receptors expressed by ipsiRGCs are both required for the targeting of ipsiRGC axons to the deep sublamina of SC. Thus, a cell–extracellular matrix (ECM) recognition mechanism specifies precise laminar targeting of ipsiRGC axons and the assembly of eye-specific parallel visual pathways.

retina | axon targeting | development | extracellular matrix | superior colliculus

Parallel pathways encode, relay, and process information about distinct stimulus properties in all sensory systems. In the visual system, information about color, contrast, object motion, and light intensity are transmitted from the retina to brain in such parallel channels by retinal ganglion cells (RGCs). Over 40 transcriptionally distinct subtypes of RGCs have been identified (1–5) and most project axons to different brain nuclei or even different regions within the same nuclei (5–10). In brain regions that process image-forming visual information, which in rodents includes the superior colliculus (SC) and dorsal lateral geniculate nucleus (dLGN), projections from distinct subtypes of RGCs are segregated into discrete sublamina. Despite this segregation being an organizing principle of parallel visual pathways in mammals, we lack an understanding of the molecular mechanisms underlying lamina-specific axon targeting.

To identify mechanisms that drive the laminar targeting of RGC axons, we focus here on the SC, the largest retinorecipient nucleus in rodents and a region responsible for driving goal-directed eye movements and a subset of innate visual behaviors (11, 12). In rodents, the majority of RGCs project axons to SC, where they arborize into the superficial-most domain in a subtype-specific fashion (5, 8). Transgenic tools labeling individual subtypes of RGCs have been instrumental in identifying lamina-specific projections from distinct RGC subtypes: for example, RGCs that convey information about object movement and direction selectivity project axons to the most superficial sublamina of SC, while α-RGCs project to deeper SC sublamina (9, 13–19). While the development of these transgenic tools has shed light on subtype-specific projection

patterns, it has long been appreciated that axons from RGCs in the contralateral eye and ipsilateral eye (contraRGCs and ipsiRGCs, respectively) targeted distinct sublamina of SC (Fig. 1 *A* and *B*) (19, 20). This segregation of eye-specific inputs is important for coordinating coherent representations of the visual field from both eyes and is considered an essential building block of binocular vision (21).

While axons from some subtypes of RGCs initially overshoot their targets or transiently innervate inappropriate brain regions during development (22, 23), axons from ipsiRGCs initially target the appropriate sublamina of the SC (24). This suggests a selective developmental mechanism drives the laminar targeting of ipsiRGC axons and generates a segregated, eye-specific parallel pathway. Here, we identified a molecularly specified extracellular matrix (ECM) ligand/cell surface receptor mechanism that patterns ipsiRGC axon targeting to the SC. Spatially restricted expression of the ECM protein Nephronectin (NPNT) is sufficient to promote the selective outgrowth of ipsiRGC axons in vitro and necessary for ipsiRGC axon targeting of SC in vivo. NPNT signals through RGD-dependent

Significance

Distinct features of the visual world are transmitted from the retina to the brain through anatomically segregated circuits. Despite this being an organizing principle of visual pathways in mammals, we lack an understanding of the signaling mechanisms guiding axons of different types of retinal neurons into segregated layers of brain regions. We explore this question by identifying how axons from the ipsilateral retina innervate a specific lamina of the superior colliculus. Our studies reveal a unique cell–extracellular matrix recognition mechanism that specifies precise targeting of these axons to the superior colliculus. Loss of this mechanism not only resulted in the absence of this eye-specific visual circuit, but it led to an impairment of innate predatory visual behavior as well.
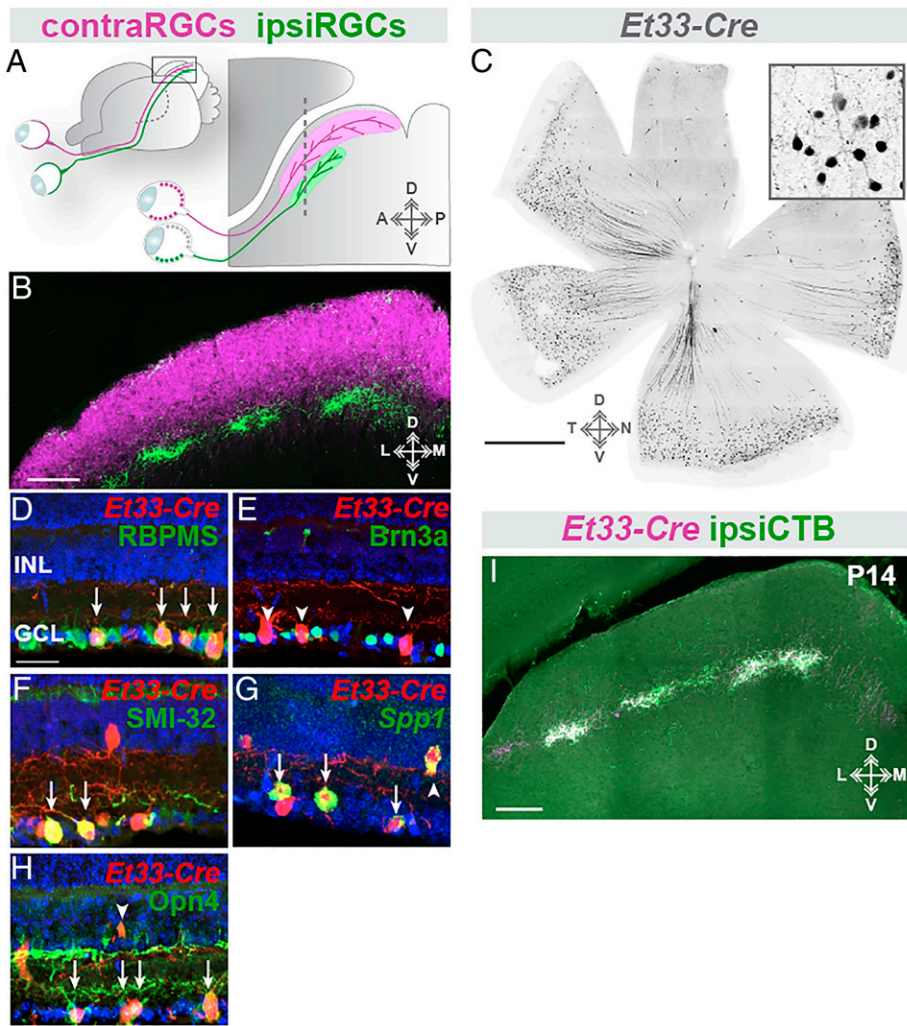
Fig. 1. ipsiRGCs innervate the deepest sublamina of retinorecipient SC. (*A*) Schematic representation of eye-specific retinocollicular projections. Dashed line approximates region of SC shown in *B* and *I*. (*B*) Coronal section depicting ipsiRGC (green) and contraRGC (magenta) projections to P14 mouse SC labeled by intraocular delivery of fluorescently conjugated CTB. (*C*) Whole-mount *Et33-Cre::Rosa-Stop-tdT* (*Et33-Cre*) retina. *Inset* shows high magnification image of tdT$^+$ RGCs. (*D–H*) Retinal cross-sections from P12 *Et33-Cre::Rosa-Stop-tdT* mice in which RGCs are labeled by IHC (*D–F*, *H*) and ISH (*G*). RBPMS labels all RGCs; Brn3A labels contraRGCs; SMI32 and *Spp1* label subsets of α-RGCs; Opn4 (Melanopsin) labels ipRGCs. Arrows highlight coexpression. Arrowheads in *E* depict tdT$^+$ RGCs that do not express Brn3a. Arrowheads in *G* and *H* depict RGCs in INL. GCL = ganglion cell layer, INL = inner nuclear layer. DAPI is shown in blue. (*I*) Coronal sections of SC show tdT$^+$ RGC axons in P14 *Et33-Cre::Rosa-Stop-tdT* mice that were monocularly injected with CTB. (Scale bar in *B*: 250 μm; in *C*: 1,000 μm for *C–G*; in *D*: 50 μm for *D–H*; in *I*: 250 μm.)

integrins and disrupting integrin signaling in ipsiRGCs (genetically or pharmacologically) impaired ipsiRGC axon growth on NPNT in vitro and impaired ipsiRGC innervation of SC in vivo. Taken together, these results shed light on a molecular matching mechanism that specifies laminar targeting of axons from the ipsilateral retina and establishes an eye-specific, parallel visual pathway.

Results

Ipsilateral-Projecting RGCs Innervate a Distinct Sublamina of Mouse SC. To label eye-specific RGC arbors in the developing SC, we delivered different fluorescently conjugated versions of cholera toxin subunit B (CTB) into each eye. Arbors of ipsiRGCs were confined to the anterior-most half of the SC and were in a deeper sublamina than arbors from contraRGCs (Fig. 1*B*). Distinct projection patterns are not the only features that differentiate ipsiRGCs and contraRGCs; in fact, these subsets of RGCs are transcriptionally distinct (25) and can therefore be distinctly labeled transgenically. Here, we show that ipsiRGCs are labeled in the *Et33-Cre::Rosa-Stop-tdT* mice (26). Not only is tdT expression restricted to the ventrotemporal crescent of retina (Fig. 1*C*) (26–28) but genetically labeled cells coexpress RNA-binding protein with multiple splicing (RBPMS; a marker of RGCs) and lack Brn3a (a marker for contraRGCs) (Fig. 1 *D* and *E*) (25, 29, 30). Approximately 2,500 RGCs are labeled in *Et33-Cre::Rosa-Stop-tdT* mice (2,631.7 ± 319.2 [SD]), equaling roughly 5% of all RGCs (31, 32), although these tdT$^+$ cells occupy space in ~30%

of the retina (31% ± 3.3 [SD], *n* = 3 retinas from 3 mice; Fig. 1*C*). tdT$^+$ RGCs expressed molecular markers associated with both α-RGCs (59.3 ± 3.4% [*n* = 668 RGCs from 3 mice] and 51.8 ± 6.1% [*n* = 317 RGCs from 3 mice] of tdT$^+$ RGCs express SMI-32 or *Spp1*, respectively) and intrinsically photosensitive RGCs (ipRGCs; 61.8 ± 3.8% [*n* = 237 RGCs from 4 mice] of tdT$^+$ RGCs express Opn4) (Fig. 1 *F–H*). As expected, central projections of *Et33-Cre::Rosa-Stop-tdT*–labeled cells targeted brain regions known to be innervated by ipsiRGCs (as well as α-RGCs and ipRGCs), including the suprachiasmatic nucleus (SCN), ventral LGN, intergeniculate leaflet, dLGN, and SC (Fig. 1*I* and *SI Appendix*, Fig. S1). Anterograde labeling of ipsiRGC projections with CTB in *Et33-Cre::Rosa-Stop-tdT* mice revealed that all tdT$^+$ RGC projections are confined to the deepest sublamina of retinorecipient SC, the region innervated by ipsiRGCs. This analysis also revealed a unique distinction in the patterns of retinorecipient innervation by ipsiRGCs. In the perinatal dLGN, ipsiRGC axons arborized broadly throughout the dLGN and were later refined to eye-specific domains by eye opening (*SI Appendix*, Fig. S1) (33). In contrast, ipsiRGC projections initially target the appropriate SC sublamina, rather than arborizing throughout the entire SC and then being refined into this sublamina (24) (see also Fig. 4*E*).

Identification of a Spatially Restricted ECM Molecule in Retinorecipient SC. Laminar targeting of axons could result from a specified molecular matching mechanism or from an activity-dependent
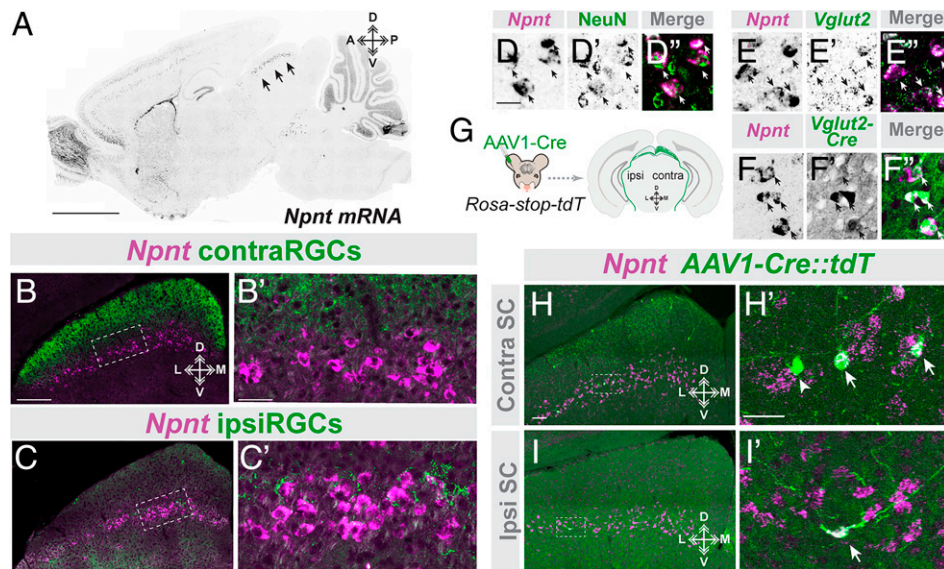
Fig. 2. NPNT is generated by retinorecipient neurons in a restricted sublamina of the developing SC. (*A*) ISH shows *Npnt* mRNA expression in a sagittal section of P8 mouse brain. Arrows highlight laminar expression of *Npnt* in SC. (*B* and *C*) ISH for *Npnt* mRNA in coronal section from P14 mouse brains in which contraRGC (*B*) and ipsiRGC (*C*) projections are labeled with CTB. *B'* and *C'* represent high magnification images of areas within dashed boxes in *B* and *C*, respectively. (*D–F*) Excitatory neurons generate *Npnt*. ISH for *Npnt* mRNA was combined with IHC for NeuN (*D*) or ISH for *Vglut2* (*E*) in P14 SC. *F* shows ISH for *Npnt* in the SC of *Vglut2-Cre::Thy1-Stop-Yfp* mice. (*G*) Schematic depiction of monocular administration of AAV1-Cre to transsynaptically label retinorecipient cells innervated by ipsi- or contraRGCs. (*H* and *I*) SC cells labeled following monocular injection of AAV1-Cre in *Rosa-Stop-tdT* mice. ISH for *Npnt* mRNA. *H'* and *I'* depict high magnification images showing expression of *Npnt* mRNA in *AAV1-Cre::Rosa-Stop-tdT* (*AAV1-Cre::tdT*)–labeled cells. (Scale bar in *A*: 1,000 μm; in *B*: 200 μm for *B* and *C*; in *B'*: 25 μm for *B'* and *C'*; in *D*: 50 μm for *D–F*; in *H*: 100 μm for *H* and *I*; and in *H'*: 50 μm for *H'* and *I'*.)

mechanism (which could include refinement or local growth). The initial specificity with which ipsiRGC axons target a segregated sublamina of SC (24) suggested to us that a genetically specified matching mechanism might underlie the assembly of eye-specific visual pathways. What might this molecular matching mechanism be? To answer this question, we screened the Allen Brain Atlas (34) for cell adhesion molecules, growth factors, morphogens, or ECM proteins whose expression was restricted to deep sublamina of the retinorecipient SC. One candidate that emerged was NPNT, an ECM glycoprotein that contains epidermal growth factor–like repeats and multiple integrin-binding motifs (35, 36). In situ hybridization (ISH) revealed *Npnt*, the gene that encodes NPNT, was absent from most regions of the neonatal and postnatal mouse brain, with two notable exceptions: a deep sublamina of SC and two distinct layers of neocortex (Fig. 2*A* and *SI Appendix*, Fig. S2). Anterograde labeling of eye-specific RGC projections with CTB revealed that *Npnt*+ cells were confined to the SC sublamina innervated by ipsiRGCs (Fig. 2 *B* and *C*). Importantly, NPNT protein was also generated by cells expressing *Npnt* transcripts and was enriched in a single lamina of the developing SC (*SI Appendix*, Fig. S2).

We next sought to identify what cells generate *Npnt*. We probed *Npnt* messenger RNA (mRNA) expression in combination with molecular and genetic approaches that label neuronal and glial cell types in the developing SC (Fig. 2 and *SI Appendix*, Fig. S2). Expression of *Npnt* was restricted to a subset of excitatory neurons that coexpressed NeuN, *Syt1*, *Vglut2*, Calb, and *Gda1* (Fig. 2 *D–F* and *SI Appendix*, Fig. S2). While NeuN, *Syt1*, *Vglut2*, and Calb were all found in larger subsets of neurons than those that generate *Npnt*, all *Gda1*+ cells coexpressed *Npnt* and therefore also appeared to represent a small subset of SC neurons confined to the deepest sublamina of retinorecipient SC (*SI Appendix*, Fig. S2). *Npnt* expression was absent from every other cell type including astrocytes, microglia, *Gad1*+ inhibitory neurons, *Sst*+ neurons, and *Pvalb*+ neurons (*SI Appendix*, Fig. S2).

Knowing that *Npnt*+ neurons are excitatory neurons (and most likely principal neurons in SC), we next asked whether these *Npnt*+ neurons are themselves retinorecipient. To test this, we used a Cre-expressing adeno-associated virus (AAV1-Cre), which delivers Cre anterogradely across a single synapse (37–39). Using a monocular delivery approach, we determined that *Npnt*+ neurons received direct input from ipsiRGCs (as well as from contraRGCs) (Fig. 2 *H* and *I*). Taken together, the structural properties of NPNT, the restriction of *Npnt*+ neurons to the sublamina of SC innervated by ipsiRGC axons, and the synaptic connections between ipsiRGCs and *Npnt*+ cells all suggest that NPNT may act as an ECM-based axonal targeting cue for ipsiRGCs.

NPNT Selectively Promotes the Growth of ipsiRGC Axons. Despite having important roles in kidney development, whether or how NPNT influences neuronal and axonal development remains unexplored. Structurally related extracellular glycoproteins have well-established roles in directing axonal guidance and targeting by their ability to bind and signal through receptors on the cell surface of the axonal growth cone. To test whether NPNT was similarly able to promote the growth of RGC axons, we turned to *in vitro* assays (Fig. 3*A* and *SI Appendix*, Fig. S3). We hypothesized that NPNT may selectively promote the outgrowth of ipsiRGC axons. Therefore, we immunopanned RGCs from neonatal *Et33-Cre::Rosa-Stop-tdT* mice. This allowed us to generate cultures containing all subtypes of RGCs with ipsiRGCs genetically labeled with tdT (*SI Appendix*, Fig. S3).

In order to test whether NPNT impacts the outgrowth of RGC axons, immunopanned RGCs were cultured on substratum containing recombinant NPNT (rNPNT) or control protein (bovine serum albumin; BSA). After 5 d, cultures were fixed and immunostained with antibodies against neurofilament (NF) to label the neurites of all RGCs. The length of NF+ neurites was similar between RGCs grown on rNPNT and control substratum, suggesting NPNT had little impact on most RGC
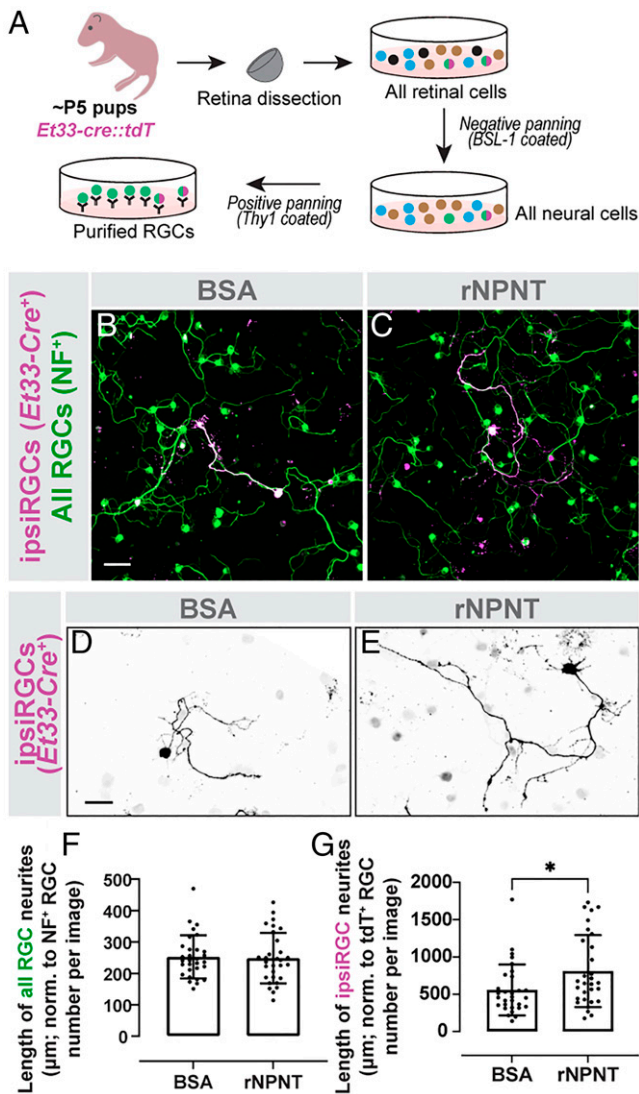
Su et al.
A cell–ECM mechanism for connecting the ipsilateral eye to the brain

PNAS | 3 of 12
https://doi.org/10.1073/pnas.2104343118

Fig. 3. NPNT promotes ipsiRGC axon outgrowth. (*A*) Schematic representation of immunopanning RGCs from neonatal *Et33-Cre::Rosa-Stop-tdT* mice. (*B* and *C*) RGCs from *Et33-Cre::Rosa-Stop-tdT* mice were cultured for 5 d on recombinant NPNT (rNPNT) or control substrates (BSA). All RGCs were labeled by IHC for NF. ipsiRGCs were identified by tdT expression (*Et33-Cre*$^+$). (*D* and *E*) High magnification of single *Et33-Cre*$^+$ RGCs on BSA or rNPNT. (*F* and *G*) Neurite outgrowth of all subtypes of RGCs (NF$^+$) or ipsiRGCs (*Et33-Cre*$^+$) was quantified measuring the total length of NF$^+$ or tdT$^+$ neurites per field of view (shown in *D* and *E*). Data were normalized to the number of NF$^+$ or tdT$^+$ RGCs per field of view. Bars represent mean ± SD. Data points represent a single field of view from a total of three experiments. In *F*, no significant differences were detected between groups by Student's *t* test. In *G*, * indicates *P* < 0.001 by Student's *t* test; *n* = 30 fields of view in BSA group and 30 fields of view in rNPNT group. (Scale bar, 75 μm for *B* and *C* and 50 μm for *D* and *E*.)

axons (Fig. 3 *B*, *D*, and *F*). In contrast, when the length of tdT$^+$ ipsiRGC neurites was measured, there was a significant increase in neurite length compared with control conditions (Fig. 3 *C*, *E*, and *G*). This suggests that NPNT specifically promotes ipsiRGC axonal growth.

NPNT Is Necessary for ipsiRGC Axon Targeting of SC. To test whether NPNT is required for retinocollicular circuit formation in vivo, we used a conditional allele to delete *Npnt* (*Npnt*$^{fl/fl}$) from select neuronal populations [to avoid its necessity in kidney development (40)]. Based on the expression of *Npnt* by

excitatory neurons in SC, we used two driver lines to delete *Npnt* expression from SC: *Nes-Cre* and *Vglut2-Cre* (*SI Appendix*, Fig. S4). The resulting mutants were viable and fertile, and the loss of NPNT from *Nes*$^+$ and *Vglut2*$^+$ cells had little impact on gross brain morphology or the cytoarchitecture of the retina or the organization of RGC axons in the optic tract (*SI Appendix*, Fig. S5). Moreover, conditional loss of *Npnt* in *Npnt*$^{fl/fl}$::*Nes-Cre* (refered to as *Nes* conditional knockout; *Nes-cKO*) and *Npnt*$^{fl/fl}$::*Vglut2-Cre* (refered to as *Vglut2-cKO*) mutants did not alter the laminar distribution of *Gda*$^+$ neurons in SC, demonstrating that NPNT was dispensable for the appropriate distribution of cells in the sublamina of SC targeted by ipsiRGC axons (*SI Appendix*, Fig. S4).

To assess eye-specific axon targeting of SC, RGC projections were anterogradely labeled by monocular injections of CTB. The loss of NPNT in both *Npnt*$^{fl/fl}$::*Nes-Cre* and *Npnt*$^{fl/fl}$::*Vglut2-Cre* had little impact on the innervation of SC by contraRGCs (Fig. 4 *A* and *B*). In contrast, the loss of NPNT in these mutants resulted in dramatic loss of ipsiRGC axons in the postnatal SC (Fig. 4 *A* and *C* and *SI Appendix*, Fig. S4). It is noteworthy that ipsiRGC axon innervation of other retinorecipient regions, such as pretectal nucleus and visual thalamus [which do not generate *Npnt* in wild-type mice but are innervated by the same cohorts of RGCs that innervate SC (5, 19)], is not altered in the absence of NPNT (Fig. 4 *A*, *D*, and *H–J*). This suggests that the absence of ipsiRGC axons in the SC of these mutants is not due to a loss of RGCs (*SI Appendix*, Fig. S5). Moreover, not only do contraRGCs projections appear normal in NPNT mutants, so do the projections from individual subtypes of contraRGCs, such as the ON–OFF direction selective RGCs (oodsRGCs) labeled in *Trhr-GFP* mice (*SI Appendix*, Fig. S4) (15). We interpret these results to suggest that SC-derived NPNT is the ECM recognition mechanism that specifies precise laminar targeting of ipsiRGC axons and the assembly of eye-specific visual pathways.

To further test this, we assessed ipsiRGC projections in neonatal *Npnt*$^{fl/fl}$::*Vglut2-Cre* mutants (and different controls). We hypothesized that ipsiRGC axons would arrive in the neonatal SC, not find the appropriate sublamina in the absence of NPNT, and then withdraw. This is indeed what we observed. At P3, ipsiRGC axons enter SC and arborize in the appropriate deepest sublamina of the retinorecipient SC (Fig. 4*E*). In contrast, in the absence of NPNT, ipsiRGC arbors appear diffuse across the entire SC (Fig. 4 *E–G*). This supports the notion that an ipsiRGC-NPNT code specifies laminar targeting of this subtype of RGC.

Since *Npnt* is expressed in subsets of amacrine cells and by infrequent cells in the ganglion cell layer (but not by ipsiRGCs labeled in *Et33-Cre::Rosa-Stop-tdT* retina or by many RGCs labeled in *Vglut2-Cre::Rosa-Stop-YFP* retina; *SI Appendix*, Fig. S2), it is possible that retinal-derived NPNT contributes to the mistargeting of ipsiRGCs in *Npnt*$^{fl/fl}$::*Nes-Cre* and *Npnt*$^{fl/fl}$::*Vglut2-Cre* mutants. To rule out the role of retina-derived NPNT in ipsiRGC targeting of SC, *Npnt*$^{fl/fl}$ mice were crossed to *Gad2-Cre* (where Cre is expressed in amacrine cells, as well as *Npnt*$^-$ GABAergic neurons in SC), *Calb2-Cre* [which is expressed in >90% of RGCs (41)], and *Et33-Cre*. In all three cases, the loss of NPNT from amacrine cells and/or RGCs had no significant impact on the targeting of ipsiRGCs to SC (Fig. 4 *A–C* and see Fig. 6*E* and *SI Appendix*, Fig. S4). These results further demonstrate the specificity and selectivity that SC-derived NPNT plays in the precise laminar targeting of ipsiRGC axons.

Integrin Signaling Is Required for ipsiRGC Targeting of SC. What might be the cell surface receptor on ipsiRGC axons that recognizes SC-derived NPNT and regulates the laminar targeting of these axons? Since NPNT was initially identified in a screen for
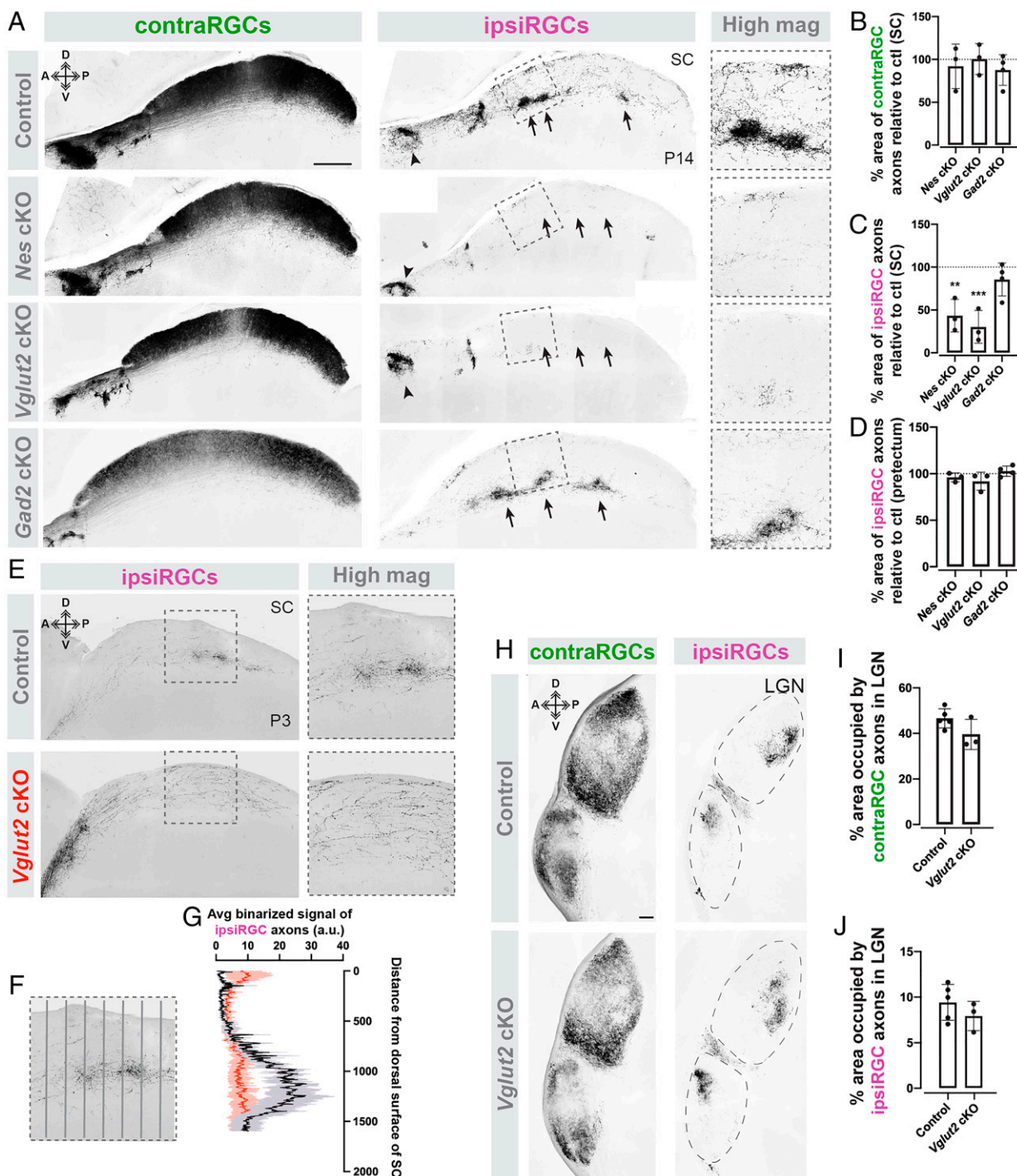
Fig. 4. NPNT is required for ipsiRGC axon innervation of SC. (*A*) CTB-labeled contra- and ipsiRGCs projections to SC in P14 control, *Npnt^fl/fl^::Nes-Cre* (*Nes* cKO); *Npnt^fl/fl^::Vglut2-Cre* (*Vglut2* cKO), and *Npnt^fl/fl^::Gad2-Cre* (*Gad2* cKO) mice. Images depict sagittal sections of SC. Arrows highlight sublamina of SC targeted by ipsiRGC axons in control and *Gad2* cKO mice, which are largely absent from *Nes* cKO and *Vglut2* cKO. Arrowheads highlight ipsiRGC axon targeting of pretectal nuclei. Boxes depict regions of ipsiRGC projections shown in high magnification panels. (*B* and *C*) Quantification of the area of SC occupied by contra- (*B*) and ipsiRGC (*C*) projections in *A* compared to three separate age-matched littermate controls for each genotype (represented by the dashed line). Bars represent means ± SD. ** indicates *P* < 0.005 and *** indicates *P* < 0.0005 when compared to control by Student's *t* test (*n* = 3 mice). (*D*) Quantification of the area of pretectum occupied by ipsiRGC projections in *A* compared to separate age-matched littermate controls (represented by the dashed line). Bars represent means ± SD. No significant difference detected between groups by Student's *t* test (*n* = 3 mice per group). (*E*) CTB-labeled ipsiRGC projections to SC in P3 control and *Npnt^fl/fl^::Vglut2-Cre* (*Vglut2* cKO) mice. Images depict sagittal sections of SC. Boxes depict regions of ipsiRGC projections shown in high magnification panels. (*F*) Schematic of line scan analysis of spatial distribution of ipsiRGC axons in SC. (*G*) Line scan analysis of spatial distribution of CTB-labeled ipsiRGC projections to SC in P3 control (black) and *Vglut2* cKO mice (red). Solid line represents mean, and shaded area represents SD (*n* = 3 animals). (*H*) CTB-labeled contra- and ipsiRGCs projections to visual thalamus (LGN) with CTB in P14 control and *Npnt^fl/fl^::Vglut2-Cre* (*Vglut2* cKO) mice. Dashed lines encircle dLGN and ventral LGN. (*I* and *J*) Quantification of the area of LGN occupied by contra- (*F*) and ipsiRGC (*G*) projections in *E* compared to age-matched controls (represented by the dashed line). Bars represent means ± SD. No significant difference detected between groups by Student's *t* test (*n* = 5 mice in control group and 3 mice in *Vglut2* cKO group).

Su et al.
A cell–ECM mechanism for connecting the ipsilateral eye to the brain

PNAS | 5 of 12
https://doi.org/10.1073/pnas.2104343118

ligands of the RGD-binding α8β1 integrin in the embryonic kidney (35, 42), a selective NPNT-integrin signaling mechanism may underlie axonal outgrowth and targeting of ipsiRGCs. To test this, we took a pharmacological approach to block integrin signaling, and we reassessed the ability of rNPNT to promote ipsiRGC axon outgrowth in vitro. Integrin signaling was blocked by treating immunopanned RGCs with integrin-blocking RGD peptides. Blocking RGD-dependent integrins in these assays reduced the ability of rNPNT to induce ipsiRGC axon outgrowth in vitro (Fig. 5 A and B).

Based on the necessity of RGD-dependent integrins for NPNT to promote ipsiRGC axon outgrowth (Fig. 3), we tested whether integrins were required for ipsiRGC innervation of SC in vivo. Function blocking RGD peptides (or control peptides) were injected into the neonatal SC as ipsiRGC axons were invading SC (Fig. 5C). Subsequently, RGC projections from both eyes were labeled with CTB. Neonatal intracollicular delivery of RGD peptides had little to no impact on contraRGCs projections (Fig. 5 D and E). In contrast, delivery of RGD peptides led to ipsiRGC axon targeting deficits similar to those observed in $Npnt^{fl/fl}$::Nes-Cre and $Npnt^{fl/fl}$::$Vglut2$-Cre mutants (Fig. 5 D and F).

These in vitro and in vivo data implicate RGD-dependent integrins in ipsiRGC axon targeting to SC, but which RGC-derived integrins serve as the receptor for NPNT remained unclear. Several transcriptional profiling studies identified distinct integrin subunits expressed in ipsiRGCs (compared to contraRGCs) (2, 25). Thus, we explored whether developing ipsiRGCs generates the β1 integrin subunit—an integrin subunit present in the most well-studied NPNT binding integrin [α8β1 integrins (35, 42)] and previously shown to play an essential role in retinotectal targeting in $Xenopus$ (43). ISH revealed a regionally restricted expression of $Itgb1$ (the gene encoding the β1 integrin subunit) in the ganglion cell layer of the developing mouse retina (Fig. 6 A and B). $Itgb1$ expression colocalized with retrogradely labeled ipsiRGCs in the ventrotemporal crescent of retina (*SI Appendix*, Fig. S6). To test whether ipsiRGCs generate $Itgb1$, we performed ISH in retinas from $Et33$-Cre mice. In the ventrotemporal retina, we observed that 41.7 ± 5.5% of $Itgb1^+$ RGCs were tdT$^+$ ipsiRGCs ($n = 84$ RGCs from 3 mice; Fig. 6C). Likewise, 82.1 ± 5.0% % of RGCs that express $Itga8^+$ were tdT$^+$ ipsiRGCs ($n = 72$ RGCs from 3 mice; Fig. 6D). Thus, developing ipsiRGCs generates the NPNT receptor. In contrast, we observed little expression of these integrin subunits in contralaterally projecting oodsRGCs labeled in $Trhr$-GFP mice (*SI Appendix*, Fig. S6).

Finally, to test whether RGC-derived β1 integrin is necessary for ipsiRGC axon targeting of SC, we crossed mice with a conditional allele of $Itgb1$ ($Itgb1^{fl/fl}$) to $Calb2$-Cre mice. Anterograde labeling with CTB was used to assess ipsiRGC and contraRGC projections to SC. While contraRGC projections in $Itgb1^{fl/fl}$::$Calb2$-Cre resembled those in littermate controls, a dramatic loss of ipsiRGC projections was observed in mutants (Fig. 6 E–G). As described above, conditional deletion of NPNT from this same population of Cre-expressing RGCs in $Calb2$-Cre mice did not lead to altered ipsiRGC targeting of SC (Fig. 6 E, H, and I). Therefore, taken together, the expression of α8β1 integrin by ipsiRGCs and the impairment of ipsiRGC axon targeting by pharmacologically and genetically blocking integrin signaling suggest that RGC-derived integrins are the receptors that recognize spatially restricted SC-derived NPNT and regulate the assembly of eye-specific, segregated visual pathways.

Loss of ipsiRGC Input to SC Disrupts Binocular Function and Impairs Innate Visual Behaviors. Although it has long been appreciated that ipsiRGCs and contraRGCs innervate adjacent, nonoverlapping sublaminae of SC, how ipsiRGCs contribute to visual
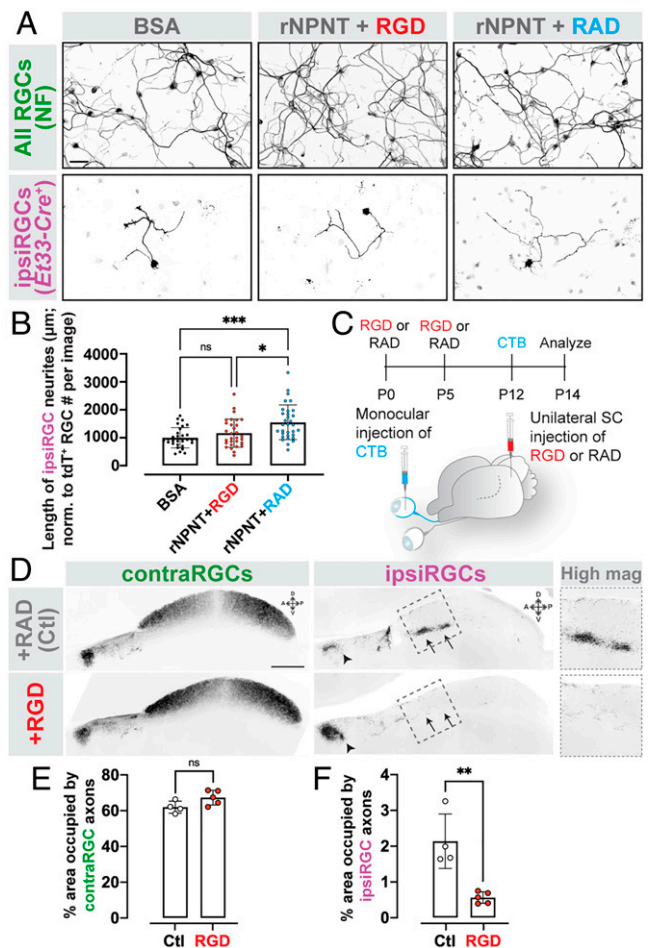
Fig. 5. RGC-dependent integrins are required for ipsiRGC innervation of SC. (*A*) RGCs from $Et33$-Cre::$Rosa$-$Stop$-tdT mice were cultured on rNPNT in the presence of integrin-blocking RGD peptides or controls (RAD). All RGCs were labeled by IHC for NF. ipsiRGCs were identified by tdT expression. (*B*) Neurite outgrowth of tdT$^+$ ipsiRGCs from A was quantified by measuring the total length of tdT$^+$ neurites. Bars represent mean ± SD. Data points represent neurites from a single tdT$^+$ ipsiRGC from a total of three experiments. * indicates $P < 0.05$, *** indicates $P < 0.0005$, and ns indicates not significant by ANOVA ($n = 30$ fields of view). (*C*) Schematic representation of intracollicular delivery of function blocking integrin peptides and intraocular delivery of CTB. (*D*) CTB-labeled contra- and ipsiRGCs projections in P14 SC that received intracollicular delivery of control peptides (RAD) or RGD peptides. Images depict sagittal sections of SC. Arrows highlight sublamina of SC targeted by ipsiRGC axons. Arrowheads highlight ipsiRGC axon targeting of pretectal nuclei. Boxes depict areas of ipsiRGC axons shown in high magnification panels. (*E* and *F*) Quantification of the area of SC occupied by contra- (*C*) and ipsiRGC (*D*) projections. Bars represent means ± SD. ** indicate $P < 0.005$ by Student's t test ($n = 4$ mice in control group, 5 mice in RGD group). No significant difference detected in comparison in *E* by Student's t test. (Scale bar in *A*: 50 μm and in *D*: 250 μm.)

function and behavior is unclear. We sought to answer this question by performing multichannel extracellular recording from neurons in the anterior SC, which receives direct retinal input from both eyes (Fig. 1A). Briefly, anesthetized mice ($Npnt^{fl/fl}$::$Vglut2$-Cre or controls) were exposed to drifting grating visual stimuli in three ocular conditions: to both eyes simultaneously or with either the ipsilateral or contralateral eye covered (Fig. 7A). In controls, as we recently reported (44), approximately one-third of SC neurons were driven monocularly (with ~64% of these being driven by the contralateral eye). The remaining SC neurons were binocularly modulated
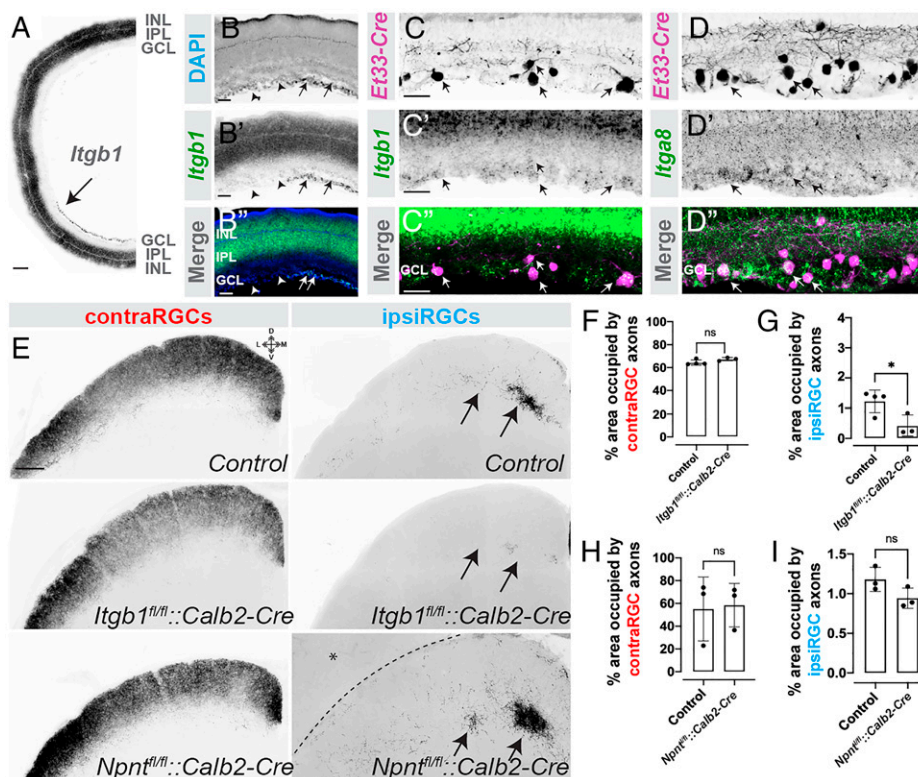
Fig. 6. β1-containing integrins are generated by ipsiRGCs and are required for ipsiRGC innervation of SC. (*A* and *B*) ISH for *Itgb1* mRNA in retinal cross-sections from P14 wild-type mice. *A* depicts a low magnification image representing almost half of the retina; *B* depicts a high magnification image of *Itgb1* mRNA and DAPI-labeled nuclei. Arrows highlight *Itgb1* expression in regionally restricted domains of the ganglion cell layer of retina. Arrowheads depict regions of the GCL without appreciable *Itgb1* expression. (*C* and *D*) ISH for *Itgb1* (*F*) and *Itga8* (*G*) mRNAs in retinal cross-sections from P12 *Et33-Cre::Rosa-Stop-tdT* mice. Arrows highlight tdT⁺ ipsiRGCs expressing these integrin subunits. (*E*) CTB labeling of contra- and ipsiRGCs projections to SC in P14 control, *Itgb1*$^{fl/fl}$*::Calb2-Cre,* and *Npnt*$^{fl/fl}$*::Calb2-Cre* mice. Images depict coronal sections of SC. Arrows highlight laminar targeting of ipsiRGC axons in control mice and their absence in *Itgb1*$^{fl/fl}$*::Calb2-Cre* mice. Dashed line depicts dorsal border of SC and asterisk depicts cortex. (*F* and *G*) Quantification of the area of SC occupied by contra- (*F*) and ipsiRGC (*G*) projections in *Itgb1*$^{fl/fl}$*::Calb2-Cre* in E. Bars represent means ± SD. ns indicates no significance, and * indicates $P < 0.05$ by Student's t test ($n = 4$ mice in control group and 3 mice in mutant group). (*H* and *I*) Quantification of the area of SC occupied by contra- (*F*) and ipsiRGC (*G*) projections in *Npnt*$^{fl/fl}$*::Calb2-Cre* in E. Bars represent means ± SD. ns indicates no significance by Student's t test ($n = 3$ mice in control group and 3 mice in mutant group). (Scale bar in *A*: 200 μm; in *B*: 50 μm; in *C*: 50 μm for *C* and *D*; and in *E*: 200 μm.)

and could be divided into four distinct response types: those neurons that respond to stimuli present to either eye or both eyes together (termed simple binocular units [BN-S]), those that respond only when stimuli were presented simultaneously to both eyes (termed emergent binocular units [BN-E]), and those that respond when one eye is covered but not when visual stimuli are presented to both eyes simultaneously (termed binocular units inhibited by the ipsilateral or contralateral eye [BN-IbI or BN-IbC, respectively]) (44) (Fig. 7*B* and *SI Appendix*, Fig. S6). Recording in *Npnt*$^{fl/fl}$*::Vglut2-Cre* mutants revealed two important differences. First, we failed to detect neurons that were monocularly driven by the ipsilateral eye (Fig. 7*C*). Second, we observed an increase in the proportion of neurons driven monocularly by the contralateral eye and therefore a decrease in the proportion of binocularly driven neurons (Fig. 7*B*). When we examined the tuning properties of the units present in *Npnt*$^{fl/fl}$*::Vglut2-Cre* mutants, we did not observe significant differences in orientation selectivity, tuning widths, or linearity of cells in the *Npnt*$^{fl/fl}$*::Vglut2-Cre* mutant SC (*SI Appendix*, Fig. S6). Taken together, the absence of neurons driven monocularly by the ipsilateral eye and the decrease in the proportion of neurons that are binocularly responsive in the *Npnt*-deficient mutants are in line with our expectation based on the dramatic loss of ipsiRGC projections to SC in these mutants.

Are direct inputs from the ipsilateral retina and binocularly responsive SC neurons important for ethologically relevant visual behaviors? Our anatomical and function studies in *Npnt*$^{fl/fl}$*::Vglut2-Cre* mutants led us to ask what role direct ipsiRGC innervation may have on SC-related innate visual behaviors. To test this, we assessed the performance of *Npnt*$^{fl/fl}$*::Vglut2-Cre* mutants (and littermate controls) in two well-established visually guided behavioral tasks: response to a looming spot (45, 46) and the prey-capture task (47, 48) (Fig. 7 *D* and *E*). Mutants lacking NPNT (and therefore ipsiRGC projections to SC) performed similar to controls in terms of freezing time, running time, hiding time, or ambulation time when presented with a dark looming stimulus (Fig. 7 *E–H*). In contrast, the ability of these mutants to capture prey was significantly impaired (Fig. 7 *J–M*). Compared to littermate controls, *Npnt*$^{fl/fl}$*::Vglut2-Cre* mutants took longer to capture prey, traveled farther during prey pursuit, and moved slower during prey pursuit (Fig. 7 *J–M*). These data suggest that direct inputs from the ipsilateral retina are critical for some, but not all, SC-mediated visual behaviors.

Discussion

Establishing precise and stereotyped cell type–specific circuits is a major challenge during brain development. Due to its accessibility, the subcortical visual system has served as a model for understanding mechanisms that underlie fundamental aspects of circuit formation: axon outgrowth and guidance, target selection, synaptogenesis, and activity-dependent

Su et al.
A cell–ECM mechanism for connecting the ipsilateral eye to the brain

PNAS | 7 of 12
https://doi.org/10.1073/pnas.2104343118
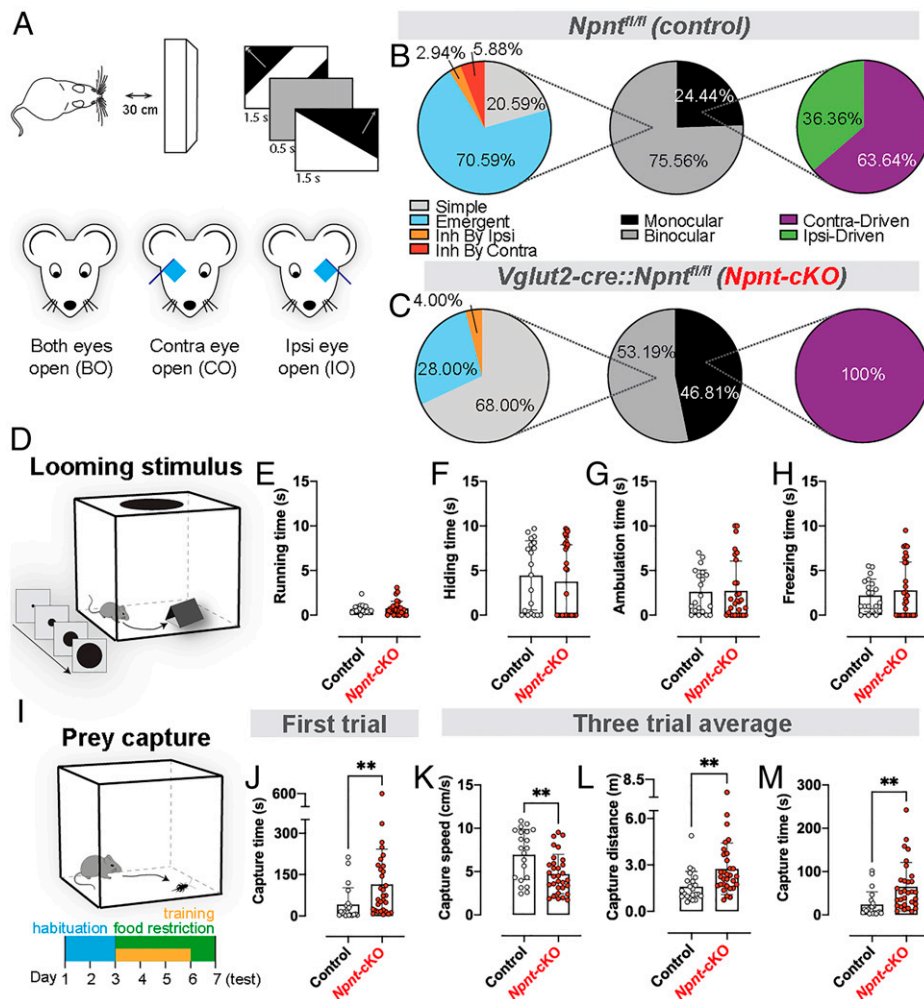
Fig. 7. ipsiRGC projections are necessary for binocular neurons and innate visual behaviors. (*A*) Schematic representation of visual stimulus paradigm in which drifting gratings were presented directly in front of mice under three ocularity conditions. (*B* and *C*) Proportions of monocular and binocular subtypes of visual neurons identified in the superior colliculi of control (*B*) and *Npnt-cKO* (*C*) mice. (*D*) Schematic representation of looming stimulus behavior assay in which an expanding dark disk is presented above the mouse in an enclosed box. (*E–H*) Quantification of different aspects of looming stimulus response behavior observed. Specifically, no significant differences in Mann–Whitney *U* tests ($n = 20$ control mice, $n = 30$ mutants) were found between control and *Npnt-cKO* mice in running time (*E*), hiding time spent in the shelter (*F*), ambulation time (*G*), and freezing time (*H*). Bars represent means ± SD, dots represent individual mice. (*I*) Schematic representation and timeline of prey-capture behavior assay in which mice hunt crickets in an enclosed box. (*J–M*) Quantification of different aspects of prey-capture behavior observed, specifically comparing control and *Npnt-cKO* mice in capture time during their first trial (*J*), then comparing capture speed (*K*), capture distance (*L*), and capture time (*M*) averaged across three trials. ** indicates $P < 0.005$ Mann–Whitney *U* test ($n = 21$ control mice, $n = 31$ mutants). Bars represent means ± SD; dots represent individual mice.

refinement. Despite considerable advances in our understanding of many of these processes, what has been lacking is a mechanism that drives individual subtypes of RGCs to project axons to regionally restricted domains of retinorecipient nuclei, which serves to parse different types of visual information into anatomically distinct parallel channels. Here, we identify a specific molecular matching mechanism that drives laminar targeting of ipsiRGC axons and establishes an eye-specific, segregated parallel visual pathway.

Cell–ECM Molecular Matching Mechanisms Underlie Laminar Targeting of RGC Axons. The assembly of cell type–specific circuits between the retina and brain relies on a combination of intrinsic transcriptional codes, cell–cell/cell–ECM interactions, and activity-dependent mechanisms (9, 10, 49–52). Focusing on ipsiRGCs, these steps include the guidance of axons from the ventrotemporal crescent of retina to the optic disk, the divergence of these axons from contraRGC at the optic tract, the

selection of retinorecipient targets, the generation of eye-specific domains (through activity-dependent refinement or through laminar targeting depending on the brain region), and the formation, maturation, and refinement of synaptic connections (31, 49, 53–55). Intrinsic transcriptional codes not only differentiate ipsiRGCs from contraRGCs (2, 25), they also provide these ipsilateral-projecting cells with a unique repertoire of cell surface receptors to respond uniquely to molecule cues as they course into the brain. Indeed, cell–cell and cell–ECM mechanisms drive the divergence of ipsiRGC axons at the optic chiasm and their homophilic fasciculation in the optic tract (27, 31, 54, 56).

Here, we add to this rich literature by revealing that a cell–ECM mechanism drives laminar targeting of ipsiRGC axons in SC. NPNT, a regionally restricted ECM glycoprotein containing epidermal growth factor–like repeats, integrin-binding motifs, and a MAM (meprin-A5 protein-receptor protein phosphatase) domain (35, 36, 42) is generated in the SC

sublamina innervated by ipsiRGCs. The protein domains of NPNT classify it as a member of an EGF-like family of adhesive glycoproteins (including laminins, thrombospondins, and tenascins). Members of this family of glycoproteins have well-documented roles in tissue development and morphogenesis, including in promoting axonal outgrowth (57, 58). Outside of the brain, NPNT plays critical roles in renal development (35, 40). Studies here now demonstrate roles for this adhesive glycoprotein in the brain, in that NPNT is sufficient to promote ipsiRGC neurite growth in vitro and is necessary for ipsiRGC innervation of SC in vivo. Thus, like has been shown for other vertebrate visual systems (59–61), an ECM glyco-code specifies precise subtype-specific laminar targeting in the mammalian retinocollicular circuit. Moreover, these results redefine the biological role of NPNT as a brain-derived laminar targeting cue.

Intrinsic differences in ipsiRGCs allow them to uniquely respond to SC-derived NPNT. A number of cell surface receptors, including integrins, are enriched in ipsiRGCs compared to other subtypes of RGCs (2, 25, 26). We now show that developing ipsiRGCs express $\alpha8\beta_1$ integrin. This integrin heterodimer was initially identified as the NPNT receptor (35) and was shown to promote axon outgrowth in vitro (62). In support of a role for this receptor in retinocollicular targeting in mice, previous studies showed that blocking β_1 containing integrins disrupts retinotectal circuit formation in *Xenopus* (43). Here, we show that disrupting integrin RGD binding with function blocking peptides impairs ipsiRGC axon growth on rNPNT in vitro and disrupts ipsiRGC innervation of SC in vivo. Genetic loss of β_1 integrins from RGCs likewise results in a loss of ipsiRGC innervation of rodent SC. Thus, integrins are necessary receptors for the laminar targeting of ipsiRGC axons in mice. This is an important difference from studies in zebrafish, which identified roles for two integrin-binding ECM molecules—CollagenIVα5 and Reelin—in retinotectal targeting (59, 61). Although both CollagenIVα5 and Reelin are capable of signaling through β_1 integrins [although not the $\alpha8\beta_1$ integrin (63, 64)], β_1 integrins are not required for the laminar targeting of RGCs in fish (59). While these differences could reflect differences in eye-specific projection patterns in these species, they may simply highlight the numerous molecular matching mechanisms necessary to pair axons from the single RGC subtypes to the correct target lamina or cells in the brain.

This raises the question of whether a unique receptor-ligand recognition mechanism is required for the laminar targeting of each RGC subtype. It is certainly possible. Loss of SC-derived NPNT impairs ipsiRGC projections to SC but not those of the oodsRGCs labeled in *Trhr-GFP* mice [Fig. 4 (15)]. It is also possible that a gradient of ECM molecules (such as NPNT) could be used to pattern the targeting of axons from multiple subtypes of RGCs in the mammalian SC. This is the case in zebrafish tectum where opposing gradients of attractive reelin and repellent Slit2 are thought to convey positional information for invading RGC axons (60, 61). Such a mechanism would greatly reduce the number of receptor-ligand recognition mechanisms to pattern laminar targeting (and similar overlapping gradients drive topographic map formation in mammalian retinorecipient zones (16, 50). Here, we show that a large subset of ipsiRGCs are α-RGCs based on the expression of *Spp1* mRNA or based on their immunoreactivity for SMI-32 (Fig. 1 *E* and *F*) (2, 65, 66). Contralateral projecting α-RGCs target SC sublamina that are just dorsal to the strata innervated by ipsiRGCs (19), so it is possible that they share some of the machinery to respond to NPNT. While a shared mechanism may drive α-RGC lamina targeting in SC, the same mechanism may not be responsible for cell type–specific circuits in other retinorecipient zones. As an example, NPNT is necessary for ipsiRGC innervation of SC but not in visual thalamus, suggesting unique

cell–ECM recognition mechanisms are required in each central target. Similar nuclei-specific difference in targeting mechanisms have been demonstrated for intrinsically photosensitive RGCs (ipRGCS), which require the ECM molecule Reelin to innervate thalamic nuclei but not the SCN (67, 68). For ipsiRGC axons, nuclei-specific roles for the teneurin family of transmembrane glycoproteins have been identified in the targeting of eye-specific domains in dLGN but not SC (69, 70). Of importance to the studies here, loss of teneurin M2 (ten_m2) does result in a reduction of the area of SC innervated by ipsiRGCs (28). Regardless of whether each synaptic lamina in SC contains unique recognition molecules or whether gradients of cues diffuse across mouse SC, it is clear that additional cell–ECM and cell–cell recognition mechanisms remain to be elucidated for a complete understanding of how cell type–specific visual circuits form in the developing mouse brain.

Multiple Pathways Convey Information from the Ipsilateral Eye to the SC. The SC is responsible for driving goal-directed eye movements and an emerging number of innate visual behaviors (45–48, 71, 72). Here, we asked whether direct input from the ipsilateral eye was required for some of these innate behaviors. Information from the ipsilateral eye would likely generate binocular responses in SC and could contribute to depth perception or to saccade-like eye movements to place objects of interest into central areas of the visual field for enhanced feature detection (12, 73), but see ref. 74. Perhaps it is not surprising then that *Npnt*-deficient mutants exhibit defects in prey capture, an ethologically relevant behavior that requires shifts in gaze to stabilize the visual scene as objects are tracked (75). This is evidence for a behavioral role of direct connections between the SC and ipsilateral eye, although another group recently reported a role for ipsiRGCs more generally in prey-capture behaviors (28). In contrast, behaviors that do not require the same precise orientations of the visual field (such as responses to looming stimulus) do not appear to require ipsiRGC innervation of SC.

While these analyses identified key roles for ipsiRGC innervation of SC in an innate behavior, functional analysis of cells in the SC of *Npnt*-deficient mice unexpectedly informed us about the circuits underlying binocularly responsive neurons. While such neurons have not been well studied in mammals with laterally oriented eyes (such as rodents), they have been in higher mammals with forward facing eyes, given the role of the SC in orienting head and eye movement in these species (76–78). It was for this reason we were surprised when we discovered that a substantial proportion of cells in the anterior mouse SC were binocularly responsive (44). Four distinct subtypes of binocularly responsive cells were identified (44). Here, we sought to explore how the responses of these cells might change in the *Npnt*-deficient mice, which lack direct innervation by ipsiRGCs. Not surprisingly, we found no cells in $Npnt^{fl/fl}::Vglut2$ mutants whose responses were driven only by the ipsilateral eye (Fig. 7). We also found a significant decrease in the proportion of binocularly responsive neurons in these mutants. However, a large number of binocularly responsive neurons remained in these mutants despite the apparent lack of ipsiRGC axons. Of course, it is possible that these responses are driven by the few ipsiRGC fibers that do remain in the SC of these mutants. However, in our opinion, the paucity of these fibers makes this seem unlikely. Instead, we interpret these results to suggest that indirect pathways may exist that transmit information from the ipsilateral eye to the SC. Such indirect pathways have been identified in postmetamorphic frogs and zebrafish, both of which lack direct ipsiRGC-SC circuits (79, 80). Thus, taken together, evidence from our anatomical, functional, and behavior studies in *Npnt*-deficient mice highlight the necessity of parsing visual information into parallel visual streams for some

Su et al.
A cell–ECM mechanism for connecting the ipsilateral eye to the brain

PNAS | 9 of 12
https://doi.org/10.1073/pnas.2104343118

NEUROSCIENCE

behaviors but also highlight that sensory systems are more complex than simple parallel pathways.

Materials and Methods

A complete description of materials and methods is available in *SI Appendix*.

Mouse Lines and Husbandry. C57BL/6 mice were obtained from Charles River Laboratories. *Pvalb-Cre*, *Nes-Cre*, *Gad2-Cre*, *Calb2-Cre*, *Vglut2-Cre*, *Sst-Cre*, *Rosa-Stop-tdT*, and *Thy1-stop-YFP* mice were obtained from Jackson Labs (stock nos. 008069, 003771, 010802, 010774, 016963, 013044, 007909). *Trhr-EGFP* mice (stock no. 030036-UCD) were obtained from Mutant Mouse Resource and Research Center (MMRRC). Conditional allele of *Npnt* (*Npnt$^{fl/fl}$*) mice were kindly from Dr. Denise K. Marciano (University of Texas Southwestern) (81). Conditional allele of *Itgb1* (*Itgb1$^{fl/fl}$*) and *Aldh1l1-EGFP* mice were provided by Dr. Stefanie Robel (Virginia Tech) (82, 83). Mice were housed in a 12-h dark/light cycle and had ad libitum access to food and water. All experiments were performed in compliance with NIH guidelines and protocols and were approved by the Virginia Polytechnic Institute and State University Institutional Animal Care and Use Committee. Please reference *SI Appendix* for more details.

Tissue Preparation and Immunohistochemistry. Fluorescent immunohistochemistry (IHC) was performed on 20-μm cryosectioned PFA-fixed brain tissue as described in refs. 67 and 84–87. Primary antibodies were diluted in blocking buffer and incubated on tissue sections overnight at 4 °C. The following antibodies and dilutions were used: mouse anti-Brn3a (diluted 1:125, Millipore), rabbit anti-RFP (diluted 1:500, Rockland), rabbit anti-Opn4 [diluted 1:2,000, Dr. C.K. Chen's laboratory (67)], mouse anti- SMI32 (diluted 1:1,000, Covance), rabbit anti-RBPMS (diluted 1:500, PhosphoSolutions), rabbit anti-GFP (diluted 1:250, Invitrogen), mouse anti-NeuN (diluted 1:200, Millipore), rabbit anti-GFAP (1:1,000, DAkoCytomation), rabbit anti-Iba1 (1:500, Wako), mouse anti-GAD67 (diluted 1:500, Millipore), rabbit anti-calbindin (diluted 1:2,500, Swant), rabbit anti-calretinin (diluted 1:2,000, Swant), mouse anti-synaptophysin (diluted 1:500, SySy), and goat anti-NPNT (diluted 1:40, R&D systems). A minimum of three animals (per genotype and per age) were compared in all IHC experiments. Please reference *SI Appendix* for more details.

Riboprobe Making and ISH. ISH was performed on 20-μm sagittal or coronal cryosectioned tissues (67, 85, 86). Antisense riboprobes were generated from full-length *Npnt* (MMM1013-202708550), *Syt1* (MM1013-9199901), *Itgb1* (MMM1013-202859073), and *Itga8* (MMM1013-202705925) Image Clones (Dharmacon) as described previously (86–88). Antisense riboprobes were generated against a 599-base pair (bp) fragment of *Sst* (corresponding to nucleotides [nt] 1 to 599 of NM_009215.1), a 973-bp fragment of *Spp1* (corresponding to nt 309 to 1279 of NM_001204201.1), a 625-bp fragment of *Gda* (corresponding to nt 1884 to 2508 of NM_010266.1), a 580-bp fragment of *Vglut2* (corresponding to nt 2190 to 2769 of NM_080853.2), and a 982-bp fragment of *Gad1* (corresponding to nt 1015 to 1996 of NM_008077.2), which were PCR-cloned into pGEM Easy T vector (Promega). Please reference *SI Appendix* for more details.

Delivery of Peptides into SC. RGD or RAD peptide injection was performed as follows. P0 mice were anesthetized with hypothermia, and the skin overlying the SC was opened and reflected. A sharp-tipped glass pipette filled with 1 μL of 100 μM RGD or RAD solution was then inserted through the thin skull and into the anterior neonatal SC. Solution within the pipette (i.e., RGD or RAD) was slowly depressed into the SC pneumatically, via a picospritzer. After 5 d (P5), mice were anesthetized a second time and were injected with the same volume, solution, and SC location. After another 7 d (P12), mice received monocular injections of Alexa Fluor 555-conjugated CTB as described previously. After 2 d, mice were euthanized, and brains were fixed in 4% paraformaldehyde. RGC projections were analyzed in 100-μm sagittal sections that were cut on a vibratome and mounted as described above.

AAV Injection. Viral tracing was done as described in ref. 38. Briefly, AAV2/1-hSyn-Cre-WPRE-hGH (2.5 × 10^{13} GC/mL, here referred to as AAV1-Cre) was used to monosynaptically label retinorecipient neurons in the SC. Briefly, mice were anesthetized with isoflurane, and 1.2 μL AAV-Cre virus was monocularly injected at an approximate 45° angle relative to the optic axis. AAV1-Cre was a gift from James M. Wilson, University of Pennsylvania (Addgene viral prep no. 105553-AAV1; RRID: Addgene_105553). Animals were euthanized and perfused with PFA as described above, 6 to 10 wk after injection.

RGC Immunopanning. We referenced the protocol outlined in ref. 89 in developing our approach to purifying and culturing RGCs. Retinas of *Et33-Cre::tdT*

(~P5) were dissected using a dissection microscope and dissociated using papain. We immunopanned RGCs from retinal suspension using Thy1.2 antibody (CD90, 1:800, Bio-RAD) and 0.02% BSA (Sigma-Aldrich) for at least 2 h at room temperature (positive panning dish). Two 15-cm Petri dishes were incubated with BSL-1 (5 μg/mL, Vector Labs) in Dulbecco's phosphate-buffered saline (D-PBS) for at least 2 h at room temperature (negative panning dishes). RGCs were detached from the dish by pipetting prewarmed RGC growth medium directly to the dish. Cells were collected by centrifuging the tube at 200 × g for 12 min at 25 °C. In total, ~70,000 cells/well were seeded in an 8-chamber slide coated with either 10 μg/mL rNPNT (R&D system), 2 μg/mL BSA, or 1X Poly-D-Lysine (Sigma-Aldrich). Chamber-slide wells were coated with rNPNT or BSA for 2 h at 37 °C before seeding cells. Medium was changed every other day. For peptide treatment, medium was changed on the second day with RGC growth medium containing either 10 μM GRGDSP or 10 μM GRADSP. After 5 d, cells were fixed for immunocytochemistry. Please reference *SI Appendix* for more details.

Electrophysiology. Visual response properties were determined as previously described (90), with minor modifications. Briefly, isoflurane-anesthetized adult mice were head fixed, and a 16-channel silicon multielectrode (Neuronexus Technologies) was inserted into at an angle of 45° to the midline and 45° to the horizontal plane through a craniotomy located ~1.5 mm lateral to the midline and ~1.5 anterior to lambda. Electrodes were labeled with 1,1'-Dioctadecyl-3,3,3',3'-Tetramethylindocarbocyanine Perchlorate (Invitrogen), and localization was confirmed post hoc via fluorescent microscopy. Multiunit signals were acquired at ~25 kHz and filtered between 0.7 to 7 kHz using a System3 Workstation (Tucker-Davis Technologies). Individual units were identified post hoc using independent components analysis. Visual stimuli were displayed on an liquid crystal display (LCD) monitor subtending ~100 × 60° of visual space and placed directly in front of the animal. Stimuli consisted of drifting square waves presented at 12 different orientations and 6 different spatial frequencies, each presented five to seven times. In addition, full-field flash and gray screens were presented to provide robust visual stimulus and determine spontaneous firing rate, respectively. Stimuli were presented in three ocular conditions: to both eyes together (both open, BO), with the ipsilateral eye covered (contralateral open, CO), and with the contralateral eye covered (ipsilateral open, IO). Based on their responsiveness under each condition, units were classified into one of seven potential types (44): monocularly driven by the contralateral eye (BO$^+$CO$^+$IO$^-$), monocularly driven by the ipsilateral eye (BO$^+$CO$^-$IO$^+$), binocular simple (BO$^+$CO$^+$IO$^+$), binocular emergent (BO$^+$CO$^-$IO$^-$), binocular inhibited by ipsilateral (BO$^-$CO$^+$IO$^-$), binocular inhibited by contralateral (BO$^-$CO$^-$IO$^+$), or binocular cross inhibited (BO$^-$CO$^+$IO$^+$).

Looming Assay. Looming stimuli were presented to the animals in white rectangular arena (47 × 37 × 30 cm) with an opaque shelter placed in a corner. Entrance of the shelter was facing the center of the arena. The arena was diffusely and evenly illuminated from above and was located within a light-proof and sound-isolated room to maintain constant environmental conditions. A camera with frame rate of 30 frames per second (FPS) for capturing mouse's behavior was secured to the stand next to the arena. All mice were tested only once to avoid a habituation to the looming stimulus. At the beginning of the test, animals were left to freely investigate the arena and the shelter for the period of 10 mins before the recording started. We started the video capturing ~10 s prior to looming stimulus, and the looming stimulus began when the animal was moving around the center of arena. Videos were recorded 10 s prior, during, and after looming stimulus. The animal's behavior was scored manually during 10 s of looming stimulus using ANY-maze software. Similar to ref. 91, we scored four types of behavior—freezing, running, hiding, and ambulation. Freezing was defined as period of one or more seconds in which the animal was completely immobile. Running was scored as activity in which the mouse started to move at least two times faster than the average speed before stimulus onset. Hiding was defined as activity when the mouse was completely hidden in the shelter. Ambulation was defined as all other locomotor activity performed in the open arena. Please reference *SI Appendix* for more details.

Prey Capture. The task was recorded in a rectangular, white acrylic arena 47 cm long × 37 cm wide × 30 cm high using the ANY-maze software. The arena was diffusely and evenly illuminated from above and was located within a light-proof and sound-isolated room to maintain constant environmental conditions. The floor of the arena was cleaned between each trial with 30% EtOH and was left to dry out completely. In order to perform this task, we followed the protocol from the study of ref. 48. Each animal in our protocol underwent a 6-d acclimation protocol followed by testing day. During testing, each mouse was given three 10-min trials to catch a cricket within

the arena. If the mouse caught the cricket within these 10 min, the trial was scored as a capture success, and the capture time for that trial was recorded. If a cricket was not captured within 10 min, the mouse was removed from the arena for 1 min and returned into the arena with a new cricket to start the next trial. Mean capture time and average speed during the hunt for each mouse on each day was calculated. All tested animals achieved 100% capture success on testing day. Please reference *SI Appendix* for more details.

Quantification and Statistical Analysis. To quantify retinal axons in SC, pretectum, and LGN, fluorescent signals in confocal micrographs were binarized using ImageJ, and the brain region was encircled to measure area and quantify the fraction of that area that is occupied by binarized signals. For RGC immunopanning, fluorescent signals (of either $Et33^+$ or NF^+ RGC neurites) were binarized in ImageJ, and the fraction of the total area of the field of view they occupied was quantified. To measure neurite length in RGC immunopanning, we measured the total length of $Et33^+$ or NF^+ neurites per field of view in ImageJ before normalizing to number of labeled RGCs in that field of view. When comparing measurements between mutants and controls, we determined statistical significance either by Student's *t* test (when comparing means between two groups) or by ANOVA or Mann–Whitney *U* test (when comparing means between three or more groups) using GraphPad Prism (version 8.0.; RRID: SCR_002798), and we indicate which test was used in the figure legends. Differences were considered significant when $P < 0.05$, and P values

are indicated in the figure legends. No data or animals were excluded from any of the analyses.

To quantify the spatial distribution of ipsiRGC axons in the SC, we used a line scan script (khatScan) in ImageJ (34), which overlays the SC with equally spaced lines along the dorsoventral axis. Binarized signals at each corresponding x coordinate of each line were averaged and plotted to show the regional distribution of ipsiRGC axons through the depth of the SC. All imaging for quantification was performed on a confocal Zeiss LSM 700 microscope at 20× magnification and 0.5 digital zoom. No data or animals were excluded from any of the analyses.

Data Availability. All study data are included in the article and/or *SI Appendix*.

1. N. M. Tran *et al.*, Single-cell profiles of retinal ganglion cells differing in resilience to injury reveal neuroprotective genes. *Neuron* **104**, 1039–1055.e12 (2019).
2. B. A. Rheaume *et al.*, Single cell transcriptome profiling of retinal ganglion cells identifies cellular subtypes. *Nat. Commun.* **9**, 2759 (2018).
3. T. Baden *et al.*, The functional diversity of retinal ganglion cells in the mouse. *Nature* **529**, 345–350 (2016).
4. J. R. Sanes, R. H. Masland, The types of retinal ganglion cells: Current status and implications for neuronal classification. *Annu. Rev. Neurosci.* **38**, 221–246 (2015).
5. E. M. Martersteck *et al.*, Diverse central projection patterns of retinal ganglion cells. *Cell Rep.* **18**, 2058–2072 (2017).
6. L. P. Morin, K. M. Studholme, Retinofugal projections in the mouse. *J. Comp. Neurol.* **522**, 3733–3753 (2014).
7. A. Monavarfeshani, U. Sabbagh, M. A. Fox, Not a one-trick pony: Diverse connectivity and functions of the rodent lateral geniculate complex. *Vis. Neurosci.* **34**, E012 (2017).
8. Y. K. Hong, C. Chen, Wiring and rewiring of the retinogeniculate synapse. *Curr. Opin. Neurobiol.* **21**, 228–237 (2011).
9. A. D. Huberman, M. B. Feller, B. Chapman, Mechanisms underlying development of visual maps and receptive fields. *Annu. Rev. Neurosci.* **31**, 479–509 (2008).
10. C. Zhang, A. L. Kolodkin, R. O. Wong, R. E. James, Establishing wiring specificity in visual system circuits: From the retina to the brain. *Annu. Rev. Neurosci.* **40**, 395–424 (2017).
11. M. A. Basso, P. J. May, Circuits for action and cognition: A view from the superior colliculus. *Annu. Rev. Vis. Sci.* **3**, 197–226 (2017).
12. S. Ito, D. A. Feldheim, The mouse superior colliculus: An emerging model for studying circuit formation and function. *Front. Neural Circuits* **12**, 10 (2018).
13. O. S. Dhande, B. K. Stafford, J. A. Lim, A. D. Huberman, Contributions of retinal ganglion cells to subcortical visual processing and behaviors. *Annu. Rev. Vis. Sci.* **1**, 291–328 (2015).
14. A. D. Huberman *et al.*, Genetic identification of an On-Off direction-selective retinal ganglion cell subtype reveals a layer-specific subcortical map of posterior motion. *Neuron* **62**, 327–334 (2009).
15. M. Rivlin-Etzion *et al.*, Transgenic mice reveal unexpected diversity of on-off direction-selective retinal ganglion cell subtypes and brain structures involved in motion processing. *J. Neurosci.* **31**, 8760–8769 (2011).
16. J. W. Triplett *et al.*, Dendritic and axonal targeting patterns of a genetically-specified class of retinal ganglion cells that participate in image-forming circuits. *Neural Dev.* **9**, 2 (2014).
17. J. N. Kay *et al.*, Retinal ganglion cells with distinct directional preferences differ in molecular identity, structure, and central projections. *J. Neurosci.* **31**, 7753–7762 (2011).
18. I. J. Kim, Y. Zhang, M. Yamagata, M. Meister, J. R. Sanes, Molecular identification of a retinal cell type that responds to upward motion. *Nature* **452**, 478–482 (2008).
19. Y. K. Hong, I. J. Kim, J. R. Sanes, Stereotyped axonal arbors of retinal ganglion cell subsets in the mouse superior colliculus. *J. Comp. Neurol.* **519**, 1691–1711 (2011).
20. P. Godement, P. Saillour, M. Imbert, The ipsilateral optic pathway to the dorsal lateral geniculate nucleus and superior colliculus in mice with prenatal or postnatal loss of one eye. *J. Comp. Neurol.* **190**, 611–626 (1980).
21. T. A. Wilks, A. R. Harvey, J. Rodger, "Seeing with two eyes: Integration of binocular retinal projections in the brain" in *Functional Brain Mapping and the Endeavor to Understand the Working Brain*, F. Signorelli, D. Chirchiglia, Eds. (InTech, Rijecka, Croatia, 2013), pp. 227–250.
22. C. A. Soares, C. A. Mason, Transient ipsilateral retinal ganglion cell projections to the brain: Extent, targeting, and disappearance. *Dev. Neurobiol.* **75**, 1385–1401 (2015).
23. J. A. Osterhout, R. N. El-Danaf, P. L. Nguyen, A. D. Huberman, Birthdate and outgrowth timing predict cellular mechanisms of axon target matching in the developing visual pathway. *Cell Rep.* **8**, 1006–1017 (2014).
24. C. García-Frigola, E. Herrera, Zic2 regulates the expression of Sert to modulate eye-specific refinement at the visual targets. *EMBO J.* **29**, 3170–3183 (2010).
25. Q. Wang, F. Marcucci, I. Cerullo, C. Mason, Ipsilateral and contralateral retinal ganglion cells express distinct genes during decussation at the optic chiasm. *eNeuro* **3**, ENEURO.0169-16.2016 (2016).
26. S. M. Koch *et al.*, Pathway-specific genetic attenuation of glutamate release alters select features of competition-based visual circuit refinement. *Neuron* **71**, 235–242 (2011).
27. A. A. Sitko, T. Kuwajima, C. A. Mason, Eye-specific segregation and differential fasciculation of developing retinal ganglion cell axons in the mouse visual pathway. *J. Comp. Neurol.* **526**, 1077–1096 (2018).
28. K. P. Johnson *et al.*, Cell-type-specific binocular vision guides predation in mice. *Neuron* **109**, 1527–1539.e4 (2021).
29. A. R. Rodriguez, L. P. de Sevilla Müller, N. C. Brecha, The RNA binding protein RBPMS is a selective marker of ganglion cells in the mammalian retina. *J. Comp. Neurol.* **522**, 1411–1443 (2014).
30. L. A. Quina *et al.*, Brn3a-expressing retinal ganglion cells project specifically to thalamocortical and collicular visual pathways. *J. Neurosci.* **25**, 11595–11604 (2005).
31. T. J. Petros, A. Rebsam, C. A. Mason, Retinal axon growth at the optic chiasm: To cross or not to cross. *Annu. Rev. Neurosci.* **31**, 295–315 (2008).
32. R. W. Williams, R. C. Strom, D. S. Rice, D. Goldowitz, Genetic and environmental control of variation in retinal ganglion cell number in mice. *J. Neurosci.* **16**, 7193–7205 (1996).
33. L. Jaubert-Miazza *et al.*, Structural and functional composition of the developing retinogeniculate pathway in the mouse. *Vis. Neurosci.* **22**, 661–676 (2005).
34. E. S. Lein *et al.*, Genome-wide atlas of gene expression in the adult mouse brain. *Nature* **445**, 168–176 (2007).
35. R. Brandenberger *et al.*, Identification and characterization of a novel extracellular matrix protein nephronectin that is associated with integrin alpha8beta1 in the embryonic kidney. *J. Cell Biol.* **154**, 447–458 (2001).
36. N. Morimura *et al.*, Molecular cloning of POEM: A novel adhesion molecule that interacts with alpha8beta1 integrin. *J. Biol. Chem.* **276**, 42172–42181 (2001).
37. B. Zingg *et al.*, AAV-mediated anterograde transsynaptic tagging: Mapping corticocollicular input-defined neural pathways for defense behaviors. *Neuron* **93**, 33–47 (2017).
38. U. Sabbagh *et al.*, Diverse GABAergic neurons organize into subtype-specific sublaminae in the ventral lateral geniculate nucleus. *J. Neurochem.* 10.1111/jnc.15101 (2020).
39. X. Xu *et al.*, Viral vectors for neural circuit mapping and recent advances in transsynaptic anterograde tracers. *Neuron* **107**, 1029–1047 (2020).
40. J. M. Linton, G. R. Martin, L. F. Reichardt, The ECM protein nephronectin promotes kidney development via integrin alpha8beta1-mediated stimulation of Gdnf expression. *Development* **134**, 2501–2509 (2007).
41. A. Kerr *et al.*, Non-cell autonomous roles for CASK in optic nerve hypoplasia. *Invest. Ophthalmol. Vis. Sci.* **60**, 3584–3594 (2019).
42. Y. Sato *et al.*, Molecular basis of the recognition of nephronectin by integrin alpha8-beta1. *J. Biol. Chem.* **284**, 14524–14536 (2009).
43. K. E. Stone, D. S. Sakaguchi, Perturbation of the developing Xenopus retinotectal projection following injections of antibodies against beta1 integrin receptors and N-cadherin. *Dev. Biol.* **180**, 297–310 (1996).
44. A. L. Russell, J. W. Triplett, Prevalence of multiple subtypes of binocularly-modulated visual neurons in the mouse superior colliculus. *bioRxiv* [Preprint] (2020). https://doi.org/10.1101/2020.12.14.422574 (Accessed 15 December 2020).
45. M. Yilmaz, M. Meister, Rapid innate defensive responses of mice to looming visual stimuli. *Curr. Biol.* **23**, 2011–2015 (2013).
46. P. Wei *et al.*, Processing of visually evoked innate fear by a non-canonical thalamic pathway. *Nat. Commun.* **6**, 6756 (2015).

Su et al.
A cell–ECM mechanism for connecting the ipsilateral eye to the brain

PNAS | 11 of 12
https://doi.org/10.1073/pnas.2104343118

NEUROSCIENCE

47. J. L. Hoy, H. I. Bishop, C. M. Niell, Defined cell types in superior colliculus make distinct contributions to prey capture behavior in the mouse. *Curr. Biol.* **29**, 4130–4138.e5 (2019).

48. J. L. Hoy, I. Yavorska, M. Wehr, C. M. Niell, Vision drives accurate approach behavior during prey capture in laboratory mice. *Curr. Biol.* **26**, 3046–3052 (2016).

49. C. Mason, N. Slavi, Retinal ganglion cell axon wiring establishing the binocular circuit. *Annu. Rev. Vis. Sci.* **6**, 215–236 (2020).

50. J. Cang, D. A. Feldheim, Developmental mechanisms of topographic map formation and alignment. *Annu. Rev. Neurosci.* **36**, 51–77 (2013).

51. H. Baier, Synaptic laminae in the visual system: Molecular mechanisms forming layers of perception. *Annu. Rev. Cell Dev. Biol.* **29**, 385–416 (2013).

52. J. R. Sanes, S. L. Zipursky, Design principles of insect and vertebrate visual systems. *Neuron* **66**, 15–36 (2010).

53. L. Erskine, E. Herrera, The retinal ganglion cell axon's journey: Insights into molecular mechanisms of axon guidance. *Dev. Biol.* **308**, 1–14 (2007).

54. J. Raper, C. Mason, Cellular strategies of axonal pathfinding. *Cold Spring Harb. Perspect. Biol.* **2**, a001933 (2010).

55. W. Guido, Development, form, and function of the mouse visual thalamus. *J. Neurophysiol.* **120**, 211–225 (2018).

56. R. Clements, K. M. Wright, Retinal ganglion cell axon sorting at the optic chiasm requires dystroglycan. *Dev. Biol.* **442**, 210–219 (2018).

57. R. O. Hynes, The extracellular matrix: Not just pretty fibrils. *Science* **326**, 1216–1219 (2009).

58. J. Engel, EGF-like domains in extracellular matrix proteins: Localized signals for growth and differentiation? *FEBS Lett.* **251**, 1–7 (1989).

59. T. Xiao, H. Baier, Lamina-specific axonal projections in the zebrafish tectum require the type IV collagen Dragnet. *Nat. Neurosci.* **10**, 1529–1537 (2007).

60. T. Xiao et al., Assembly of lamina-specific neuronal connections by slit bound to type IV collagen. *Cell* **146**, 164–176 (2011).

61. V. Di Donato et al., An attractive reelin gradient establishes synaptic lamination in the vertebrate visual system. *Neuron* **97**, 1049–1062.e6 (2018).

62. U. Müller, B. Bossy, K. Venstrom, L. F. Reichardt, Integrin alpha 8 beta 1 promotes attachment, cell spreading, and neurite outgrowth on fibronectin. *Mol. Biol. Cell* **6**, 433–448 (1995).

63. J. Khoshnoodi, V. Pedchenko, B. G. Hudson, Mammalian collagen IV. *Microsc. Res. Tech.* **71**, 357–370 (2008).

64. L. Dulabon et al., Reelin binds alpha3beta1 integrin and inhibits neuronal migration. *Neuron* **27**, 33–44 (2000).

65. L. A. Laboissonniere et al., Molecular signatures of retinal ganglion cells revealed through single cell profiling. *Sci. Rep.* **9**, 15778 (2019).

66. B. Lin, S. W. Wang, R. H. Masland, Retinal ganglion cell type, size, and spacing can be specified independent of homotypic dendritic contacts. *Neuron* **43**, 475–485 (2004).

67. J. Su et al., Reelin is required for class-specific retinogeniculate targeting. *J. Neurosci.* **31**, 575–586 (2011).

68. J. Su, M. A. Klemm, A. M. Josephson, M. A. Fox, Contributions of VLDLR and LRP8 in the establishment of retinogeniculate projections. *Neural Dev.* **8**, 11 (2013).

69. N. Dharmaratne et al., Ten-m3 is required for the development of topography in the ipsilateral retinocollicular pathway. *PLoS One* **7**, e43083 (2012).

70. C. A. Leamey et al., Ten_m3 regulates eye-specific patterning in the mammalian visual pathway and is required for binocular vision. *PLoS Biol.* **5**, e241 (2007).

71. D. L. Sparks, C. Lee, W. H. Rohrer, Population coding of the direction, amplitude, and velocity of saccadic eye movements by neurons in the superior colliculus. *Cold Spring Harb. Symp. Quant. Biol.* **55**, 805–811 (1990).

72. F. Liang et al., Sensory cortical control of a visually induced arrest behavior via corticotectal projections. *Neuron* **86**, 755–767 (2015).

73. A. F. Meyer, J. O'Keefe, J. Poort, Two distinct types of eye-head coupling in freely moving mice. *Curr. Biol.* **30**, 2116–2130.e6 (2020).

74. J. M. Samonds, V. Choi, N. J. Priebe, Mice discriminate stereoscopic surfaces without fixating in depth. *J. Neurosci.* **39**, 8024–8037 (2019).

75. A. M. Michaiel, E. T. Abe, C. M. Niell, Dynamics of gaze control during prey capture in freely moving mice. *eLife* **9**, e57458 (2020).

76. N. Berman, M. Cynader, Comparison of receptive-field organization of the superior colliculus in Siamese and normal cats. *J. Physiol.* **224**, 363–389 (1972).

77. M. E. Goldberg, R. H. Wurtz, Activity of superior colliculus in behaving monkey. I. Visual receptive fields of single neurons. *J. Neurophysiol.* **35**, 542–559 (1972).

78. E. C. Dias, C. E. Rocha-Miranda, R. F. Bernardes, S. L. Schmidt, Disparity selective units in the superior colliculus of the opossum. *Exp. Brain Res.* **87**, 546–552 (1991).

79. S. B. Udin, Binocular maps in Xenopus tectum: Visual experience and the development of isthmotectal topography. *Dev. Neurobiol.* **72**, 564–574 (2012).

80. C. Gebhardt et al., An interhemispheric neural circuit allowing binocular integration in the optic tectum. *Nat. Commun.* **10**, 5471 (2019).

81. S. E. Zimmerman et al., Nephronectin regulates mesangial cell adhesion and behavior in glomeruli. *J. Am. Soc. Nephrol.* **29**, 1128–1140 (2018).

82. S. Robel et al., Conditional deletion of beta1-integrin in astroglia causes partial reactive gliosis. *Glia* **57**, 1630–1647 (2009).

83. A. J. Potocnik, C. Brakebusch, R. Fässler, Fetal and adult hematopoietic stem cells require beta1 integrin function for colonizing fetal liver, spleen, and bone marrow. *Immunity* **12**, 653–663 (2000).

84. M. A. Fox et al., Distinct target-derived signals organize formation, maturation, and maintenance of motor nerve terminals. *Cell* **129**, 179–193 (2007).

85. J. Su et al., Paracrine role for somatostatin interneurons in the assembly of perisomatic inhibitory synapses. *J. Neurosci.* **40**, 7421–7435 (2020).

86. J. Su et al., Collagen-derived matricryptins promote inhibitory nerve terminal formation in the developing neocortex. *J. Cell Biol.* **212**, 721–736 (2016).

87. J. Su, K. Gorse, F. Ramirez, M. A. Fox, Collagen XIX is expressed by interneurons and contributes to the formation of hippocampal synapses. *J. Comp. Neurol.* **518**, 229–253 (2010).

88. A. Monavarfeshani et al., LRRTM1 underlies synaptic convergence in visual thalamus. *eLife* **7**, e33498 (2018).

89. A. Winzeler, J. T. Wang, Purification and culture of retinal ganglion cells from rodents. *Cold Spring Harb. Protoc.* **2013**, 643–652 (2013).

90. R. B. Kay, J. W. Triplett, Visual neurons in the superior colliculus innervated by Islet2+ or Islet2− Retinal ganglion cells display distinct tuning properties. *Front. Neural Circuits* **11**, 73 (2017).

91. L. D. Salay, N. Ishiko, A. D. Huberman, A midline thalamic circuit determines reactions to visual threat. *Nature* **557**, 183–189 (2018).

12 of 12 | PNAS
https://doi.org/10.1073/pnas.2104343118

Su et al.
A cell–ECM mechanism for connecting the ipsilateral eye to the brain